# Neural Network Sampling of the Free Energy Landscape for Nitrogen Dissociation on Ruthenium

*Elizabeth M. Y. Lee,[1,‡] Thomas Ludwig,[2,3,‡] Boyuan Yu,[1] Aayush R. Singh,[2,†]*

*François Gygi,[4] Jens K. Nørskov,[2,3,5]* and Juan J. de Pablo[1,6]**

[1]Pritzker School of Molecular Engineering, The University of Chicago, Chicago, Illinois 60637, USA

[2]SUNCAT Center for Interface Science and Catalysis, Department of Chemical Engineering, Stanford University, Stanford, California 94305, United States

[3]SUNCAT Center for Interface Science and Catalysis, SLAC National Accelerator Laboratory, 2575 Sand Hill Road, Menlo Park, California 94025, United States

[4]Department of Computer Science, University of California, Davis, California 95616, USA

[5]Department of Physics, Technical University of Denmark, Lyngby 2800, Denmark

[6]Argonne National Laboratory, 9700 Cass Avenue, Lemont, IL 60439, USA.

[‡]These authors contributed equally

**Corresponding Authors**

*Emails: jkno@dtu.dk (J.K.N.); depablo@uchicago.edu (J.J.d.P.)

ABSTRACT: In heterogeneous catalysis, free energy profiles of reactions govern the mechanisms, rates, and equilibria. Energetics are conventionally computed using the harmonic approximation (HA), which requires determination of critical states *a priori*. Here, we use neural networks to efficiently sample and directly calculate the free energy surface (FES) of a prototypical heterogeneous catalysis reaction—the dissociation of molecular nitrogen on ruthenium—at density functional theory-level accuracy. We find vibrational entropy of surface atoms, often neglected in HA for transition metal catalysts, contributes significantly to the reaction barrier. The minimum free energy path for dissociation reveals an "on-top" adsorbed molecular state prior to the transition state. While a previously reported flat-lying molecular metastable state can be identified in the potential energy surface, it is absent in the FES at relevant reaction temperatures. These findings demonstrate the importance of identifying critical points self-consistently on the FES for reactions that involve considerable entropic effects.

TOC GRAPHIC:

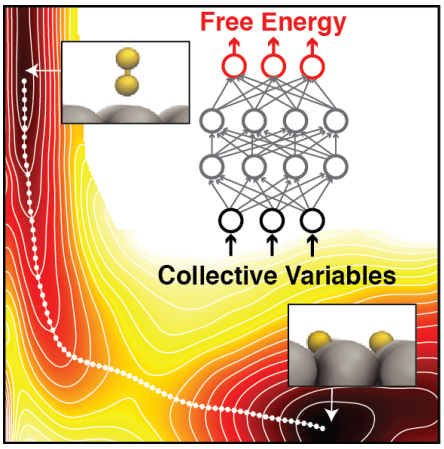


KEYWORDS: heterogeneous catalysis, chemical reactions, free energy, *ab initio* molecular dynamics, enhanced sampling, artificial neural networks

Reactions of molecules on solid surfaces are the basis for many industrial chemical processes, including semiconductor processing, corrosion, electrochemistry, and heterogeneous catalysis.[1–3] A central industrial process in heterogeneous catalysis is ammonia synthesis.[4,5] On ruthenium, one of the most active catalysts for ammonia synthesis, the rate-determining step is the dissociation of molecular nitrogen.[6] There have been numerous experimental and theoretical studies on the energetics of this process. Surface science techniques such as reactive scattering, molecular beam, and laser-assisted associated desorption have measured dissociation probabilities and energy barriers of $N_2$ on Ru(0001).[7–12] For these surface catalytic reactions, density functional theory (DFT) is widely used to predict reaction energies and activation barriers.[2,13–19]

Early DFT studies of $N_2$ on Ru(0001) have computed dissociation free energy barriers based on normal mode analysis with the harmonic approximation (HA) and showed reasonable agreement with thermal rate experiments.[6] These calculations require the predetermination of local minima and transition states of the potential energy surface (PES) but do not capture anharmonic contributions. Within surface science, a standard practice for computing free energies is to use a single, lowest-energy configuration for each critical state and the normal modes of only the adsorbed atoms (*i.e.*, adsorbate) excluding the surface atoms. However, recent theoretical and experimental investigations of larger reacting molecules or structurally complex catalytic materials, like metal organic frameworks (MOFs), have reported appreciable entropic contributions to the reaction barriers and rates beyond standard HA, such as configurational multiplicity and anharmonicity.[20–24] These findings suggest that extending free energy calculations beyond the conventional harmonic approach[25] is essential for predicting free energy barriers and determining the reactive configurations.

While the free energies of surface reactions at finite temperature and pressure can be directly calculated from dynamical simulations using DFT, *i.e.*, *ab initio* molecular dynamics (AIMD), these simulations are computationally demanding (*e.g.*, several hundred electrons) and limited to short-time scales (*e.g.*, tens to hundreds of picoseconds). Recent works on $N_2$ on Ru and other molecule-surface reactions have circumvented this problem by replacing DFT with neural networks and other machine-learning-based PES[15,26] or empirical interatomic potentials[27,28]. Here we develop and apply an enhanced sampling approach to map the free energy landscape of $N_2$ undergoing molecular dissociation on Ru using AIMD. In this approach, we compute potential energies and forces directly from DFT, so the PES part of the free energy surface (FES) is constructed by performing "on-the-fly" DFT calculations.

Enhanced sampling methods enable the efficient calculation of the potential of mean force (PMF) or the FES along the reaction coordinate by accelerating dynamic simulations. Adaptive enhanced sampling methods, such as metadynamics[29] and adaptive biasing force (ABF)[30], explore the configurational space by adding an adaptively computed bias to the original dynamics. Until recently[22,25,31–40], these approaches focused on classical systems[41–43] with few surface chemistry applications. In the last two years, machine learning-assisted enhanced sampling methods have been introduced to accelerate sampling efficiency over existing methods.[44–50] The combined-force frequency (CFF) approach[45] uses Bayesian regularized artificial neural networks (BRANN) to represent the bias based on the PMF and its gradient, combining several concepts from existing methods, such as metadynamics and ABF. However, the generalizability of these emerging methodologies to reactive systems on materials modeled with electronic structure calculations has not yet been demonstrated.

In this work, we present a DFT description of the PMF for dissociation of $N_2$ on Ru(0001)

using a neural network-based enhanced sampling method called CFF with AIMD (i.e., CFF-AIMD). We show that neural networks accelerate enhanced sampling simulations to predict the long-timescale surface reaction phenomenon using AIMD. We find that the entropies of the intermediate states affect the topology of the FES, which consequently deviates from the PES. We use several variants of HA to show that the computed PMF using CFF-AIMD captures temperature-dependent contributions to the free energies that are not included in conventional HA methods, such as the effects of multiple dissociated states, configurational degeneracies, and vibrational entropy of surface atoms. We demonstrate that these entropic effects can be critical for predicting the free energies and barriers for reactions on metal surfaces.

Free energy calculations with enhanced sampling simulations are less computationally demanding than using unbiased AIMD but can require a large number of DFT calculations to converge sampling statistics and quantify statistical uncertainties. Therefore, we adopt a computationally efficient DFT model, consisting of a $2 \times 2$ unit cell of an $N_2$ molecule on a two-layer Ru(0001) surface (Figure 1A) (see Computational Methods). In CFF-AIMD simulations, we use two-dimensional (2D) collective variables (CVs) to describe the bond breaking/formation and adsorption/desorption processes for the dissociation of $N_2$ on Ru: the N-N distance ($r$) and the molecule-surface distance ($Z$) (Figure 1A). An ensemble of final dissociated states (2N*) can be sampled because there are two stable N* adsorption sites: hexagonal close-packed (HCP) hollow and face-centered cubic (FCC) hollow sites, which differ in the presence of a ruthenium atom in the layer below the HCP hollow site (Figure 1B). In total, we performed ~500 ps of enhanced sampling simulations using multiple walkers or replicas, amounting to ~17 million timesteps (see Table S2 for a summary of simulations performed in this work).

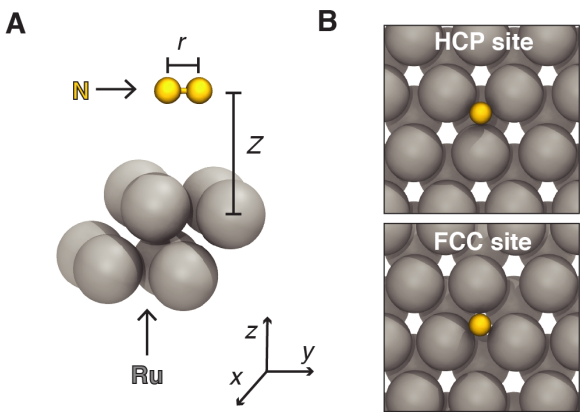


**Figure 1.** Schematic of the molecular dissociation on Ru(0001). (A) The system is modeled as a nitrogen molecule on a 2x2 unit cell of a two-layer Ru(0001) slab with 3D periodic boundary conditions. Two CVs are used to perform enhanced sampling simulations: $r$ (N-N distance) and $Z$ (molecule-surface distance projected along the $z$-coordinate). (B) There are two stable adsorption sites for nitrogen atoms: HCP and FCC hollow sites. These two sites give rise to an ensemble of possible 2N* states, including HCP-HCP, FCC-FCC, and HCP-FCC configurations.

As demonstrated in Figures 2A-2C, CFF-AIMD successfully samples the configurational space describing the nitrogen dissociation reaction. Using 16 walkers at 1400 K, CFF-AIMD identifies the initial ($N_2$*) and final states (2N*) of the surface reaction, respectively. By applying the nudged elastic band (NEB) method[51] to the BRANN-fitted FES (Supporting Information), we find the minimum free energy path (MFEP) between the adsorbed molecular state ($N_2$*) minimum at $(r, Z)$ = (1.1, 2.7) Å, where the molecular axis is nearly perpendicular to the surface (the on-top configuration), and the dissociated atomic state (2N*) minimum at $(r, Z)$ = (2.7, 1.1) Å, where nitrogen atoms adsorb to predominantly HCP hollow sites. This MFEP has a sharp curvature with a narrow passage connecting $N_2$* and the transition state (TS) (Figure 3C).

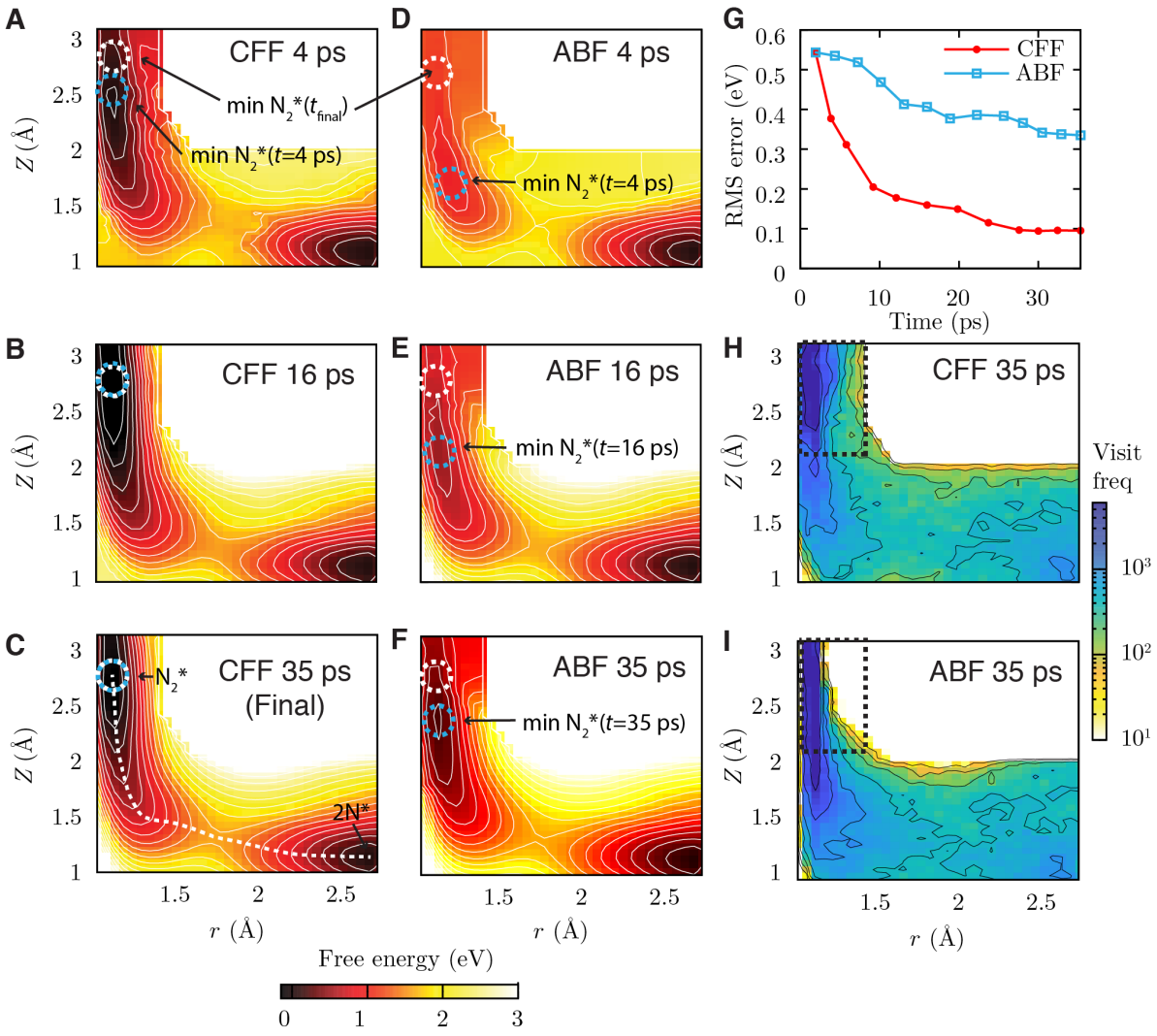


**Figure 2.** Comparison of two similar enhanced sampling simulation methods with and without neural networks (CFF and ABF). (A-C) 2D FES data from a CFF-AIMD simulation at 1400 K. White and blue circles represent the final converged minima of the $N_2$* state and the instantaneous free energy minima during the simulation, respectively. CFF correctly identifies the two minima ($N_2$* and 2N*) within 16 ps of simulation time and is terminated after 35 ps using 16 walkers once the CV space is fully sampled and the root-mean-squared (RMS) error of less than 0.1 eV is reached (see panel **G**). The final FES reveals a dissociation pathway having a narrow transition region and a sharp curve, indicated by the MFEP (white dashed line). (D-F) 2D FES data from an ABF-AIMD simulation at 1400 K. ABF predicts the minimum for the $N_2$* state incorrectly within the same simulation time as CFF. (G) Changes in the RMS error in free energies, relative to a long independent simulation, over the simulation time (see Supporting Information for the details). CFF converges several times faster than ABF, showing that the use of neural network representation accelerates sampling. (H, I) Biased distributions from CFF-AIMD and ABF-AIMD simulations. ABF insufficiently samples configurations in the $N_2$* region (inside the black box), leading to an unconverged PMF in panel **F**. In contrast, CFF samples configurations more uniformly in the entrance region, where ABF underperforms.

To examine how neural networks accelerate free energy calculations for surface reactions, we also perform simulations using an enhanced sampling method without neural networks: ABF-AIMD. ABF is chosen to mimic the adaptive sampling strategy in CFF without the improvements brought forth by neural networks (see Supporting Information on the CFF method description).

CFF-AIMD converges to the underlying FES faster than ABF-AIMD (Figures 2A-2G). ABF-AIMD does not converge after extensive simulations (~102 ps) (see Figure S7C). Regions proximal to the $N_2$* state, which contains sharp free energy differences (~2 eV) over a narrow range of configurational space ($r = 1.1—1.5$ Å , $Z = 2—3$ Å), are undersampled (see Figure 2I). Specifically, ABF relies on determining the force a molecular system experiences along an order parameter and adds an opposing force (the bias) in an iterative fashion, such that the total force is zero.[30] This iterative process is particularly slow across large free energy barriers (e.g., the configuration space proximal to $N_2$*), where sampling is too sparse to obtain accurate estimates of the forces that arise from the underlying FES (see the Supporting Information on ABF-AIMD). In contrast, our CFF-AIMD method directly approximates the global FES using neural networks based on the potential energy and forces computed from on-the-fly DFT calculations. CFF-AIMD arrives at more accurate estimates of the biasing forces required by interpolating the free energies between both sparsely-sampled and well-sampled configurations at each iteration (see also the Supporting Information Sec. 5.1). These combined effects lead to a faster convergence as well as a more uniform sampling with CFF-AIMD compared to ABF-AIMD (Figures 2H-2I), thereby highlighting the ability of the CFF-AIMD method to efficiently and accurately sample free energy landscapes containing narrow valleys and sharp curvatures, which are common in molecular dissociation on surfaces[52,53].

In order to understand the dissociation reaction mechanism, we analyze the trajectories from CFF-AIMD simulations. Snapshots of the surface dissociation reaction process are shown in Figure 3A, and the full process is shown in Movie S1. Initially, the molecular nitrogen adsorbs to the metal with its molecular axis nearly perpendicular to the surface, with an average tilt angle of $\phi$=16° (state $N_2$*), as seen in the angular distribution, $P(\phi)$, plotted in Figure 3B. Thermal rotation causes this on-top configuration to bend toward the surface (state A) and lie flat as $\phi$=90° (state M). As the N-N bond stretches, the adsorbate reaches a transition state, where, on average, one nitrogen atom is near an HCP hollow site, while the other approaches the closest FCC hollow site. The other nitrogen atom diffuses to an empty hollow site and the N-N bond breaks. At 700 K, nearly all dissociated nitrogen atoms adsorb to HCP hollow sites (HCP-HCP), the lowest-energy 2N* state predicted from DFT calculations. However, as temperature increases to 1400 K, the nitrogen complex at the transition state dissociate into other 2N* states as well, such as HCP-FCC and FCC-FCC configurations. The fraction of HCP-FCC and FCC-FCC configurations that overlap with the 2N* state minimum increases with increasing temperature, based on calculations using a Delaunay triangulation-based adsorption site analysis[54,55] (Figure S11). These results suggest that there are multiple reaction pathways for $N_2$ dissociation on Ru(0001) at high temperatures.

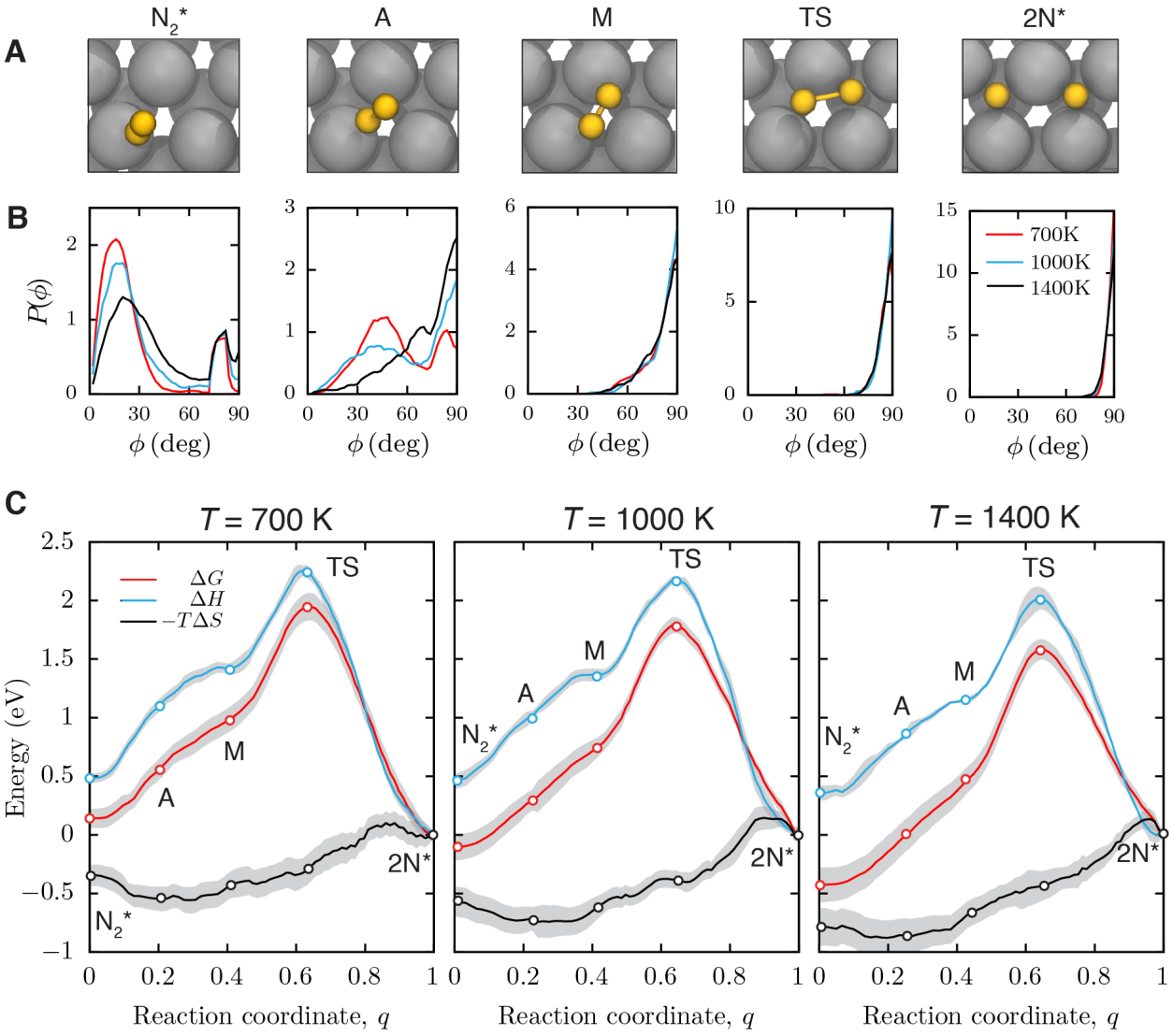


**Figure 3.** Temperature-dependent free energy landscapes for the dissociation reaction. (A) A series of snapshots from part of a CFF-AIMD trajectory at 700 K showing changes in the adsorbate configuration as the nitrogen molecule dissociates on Ru(0001): the on-top molecular state ($N_2$*), tilted adsorbed state (A), flat-lying molecular state (M), transition state (TS), and dissociated state (2N*) at the free energy minimum. (B) Probability distributions of the title angle between the N-N bond and the surface normal (see details of the calculation in the Supporting Information). Molecularly adsorbed states rotate about the molecular axis at high temperatures. (C) 1D free energy, enthalpic, and entropic profiles, referenced to the 2N* state. Entropies of adsorbates states are non-uniform along the reaction coordinate. Reaction free energies (at $q$=$N_2$*) and surface reaction barriers (at $q$=TS) change with the reaction temperature. The local minimum in $\Delta H(q)$ corresponding to state M is absent in $\Delta G(q)$.

To compute the barrier for dissociative adsorption, *i.e.*, $\Delta G = G(\mathrm{TS}) - G(\mathrm{N_{2\,gas}})$,[12,56] we reference relative free energies of adsorbed states from CFF-AIMD to the gas phase, assuming ideal gas behavior for the reference state and HA for the 2N* state (see Supporting Information). Increasing the reaction temperature appreciably raises the dissociation adsorption free energy barrier from 2.02 ± 0.12 eV at 700 K to 2.75 ± 0.09 eV at 1400 K, mainly because the gas phase has higher entropy than the adsorbed state. Laser-assisted associative desorption experiments have reported the barrier to be ~1.8 to 2.1 eV for samples with ~23 to 48 % nitrogen coverage.[12] A recent quasi-classical simulation study based on DFT has determined that a barrier of 1.8 eV is consistent with scattering experiments.[15] Calculated barriers using CFF-AIMD at 700 K (2.02 ± 0.12 eV) are in reasonable agreement with available experimental data within a few tenths of eV. Discrepancies can be due to the exchange-correlational functional in DFT,[57,58] the surface coverage of nitrogen atoms,[12] and other possible physical effects, such as non-adiabatic dynamics[16] and surface expansion[15].

In designing catalysts and reaction processes using microkinetic models, energetics of intermediates and transition states are used to predict chemical kinetics.[59] The computed 1D- and 2D-PMFs for the surface dissociation reaction and the enthalpic and entropic contributions are shown in Figures 3C and 4. The surface reaction free energy, $\Delta G_r = G(\mathrm{2N^*}) - G(\mathrm{N_2^*})$, increases from -0.14 eV to 0.43 eV as temperature increases from 700 K to 1400 K. At low temperature, the surface dissociation reaction favors the product (2N*) while at high temperature, the equilibrium is shifted towards the reactant ($N_2$*). The predicted activation energy for associative desorption, $\Delta G^{\ddagger} = G(\mathrm{TS}) - G(\mathrm{2N^*})$, decreases from 1.94 eV at 700 K to 1.66 eV at 1400 K. The transition state has higher entropy than the 2N* state ($\Delta S^{\ddagger} > 0$), while the activation enthalpy ($\Delta H^{\ddagger}$) decreases with temperature due to the greater population of higher-enthalpy dissociated states with

increasing temperature. Therefore, the combined effect from enthalpic and entropic contributions causes $\Delta G^{\ddagger}$ to decrease at higher temperature.

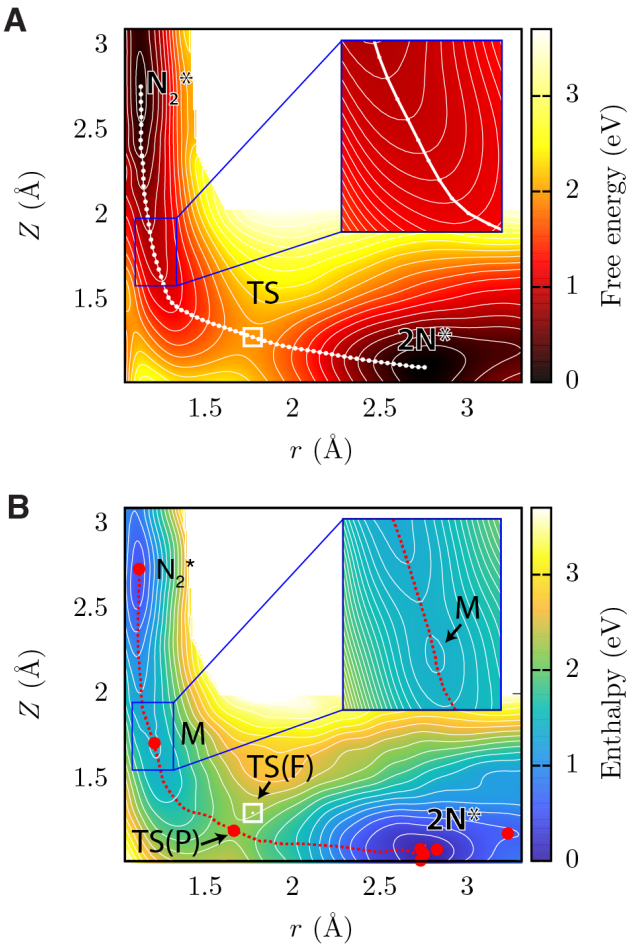


**Figure 4.** Intermediate states and minimum energy paths of the potential and free energy surfaces. (A) 2D PMF, $\Delta G(r, Z)$, relative to the 2N* state, computed from CFF-AIMD simulations at 700 K. Only three critical points ($N_2$*, TS, and 2N* states in white square markers) are identified along the MFEP (white line). (B) Average potential energy or enthalpic contribution to the free energy, $\Delta H(r, Z)$, of the same system as in panel (A). Critical points on the PES found from energy minimization and transition state search methods (in red circles) coincide well with the topology of $\Delta H(r, Z)$, The minimum potential energy path computed from $\Delta H(r, Z)$ indicates that the TS on the PES (in red circle) lies closer to the surface than the TS on the FES (in white square marker). Inset figures are zoomed views near state M predicted from energy minimization. While a local minimum corresponding to state M is found in $\Delta H(r, Z)$, it is absent in $\Delta G(r, Z)$. The energy difference between successive contour lines is 0.2 eV in main figures and 0.05 eV in inset figures.

In addition to the energetics, we find differences in the critical points between FES and PES. Critical points on the PES were identified using energy minimization and transition state search methods (see the Computational Methods). A shallow local energy minimum corresponding to state M that is also predicted from energy minimization, is seen ~1 eV above the $N_2$* state in averaged potential energy (or enthalpic) profiles computed from CFF-AIMD (Figures 3C and 4B). This intermediate precursor state has been described in previous works as an additional metastable molecularly adsorbed state along the minimum energy path.[14] Interestingly, this minimum is absent in 1D- and 2D-PMFs (Figures 3C and 4A). Thus, state M is not a true metastable state within our model at the temperatures studied. These results indicate that entropic effects play a critical role in the thermal stability of intermediate precursors at finite temperatures. In nitrogen dissociation, the energetics and locations of precursors along the MFEP may affect the scattering dynamics over multiple metal surfaces, *e.g.,* Ru(0001) and Cu(111).[9,60] Moreover, the presence of precursor states has been hypothesized to influence reaction kinetics in a variety of other surface reactions (*e.g.,* formic acid oxidation).[61] We also find that entropy causes a shift in the MFEP (Figure 4A) relative to the minimum potential energy path (Figure 4B). Consequently, the transition state from CFF-AIMD lies further away from the Ru surface by ~0.1 Å than what is predicted from the PES-based transition state search methods (see Computational Methods). Methods using critical points in the PES to predict free energy diagrams assume that entropy plays a minor role in determining intermediate and transition states. Our findings suggest the merit of directly identifying critical points from the FES, especially for systems with significant entropic effects.

To understand the origins of temperature-dependent contributions to the energetics of the reaction process, we compare findings from CFF-AIMD simulations to those from HA (Figure 5), which uses critical points of the PES and captures the vibrational entropy and enthalpy based on

normal-mode analysis, zero-point vibrational energy (ZPE) effects, and configurational entropy (see Computational Methods). As seen in Table S1, there is a good agreement in HA results using quantum and classical harmonic approximation for this reaction at the temperatures studied in this work, providing evidence that quantum effects such as ZPE do not substantially affect the comparisons made in this work.

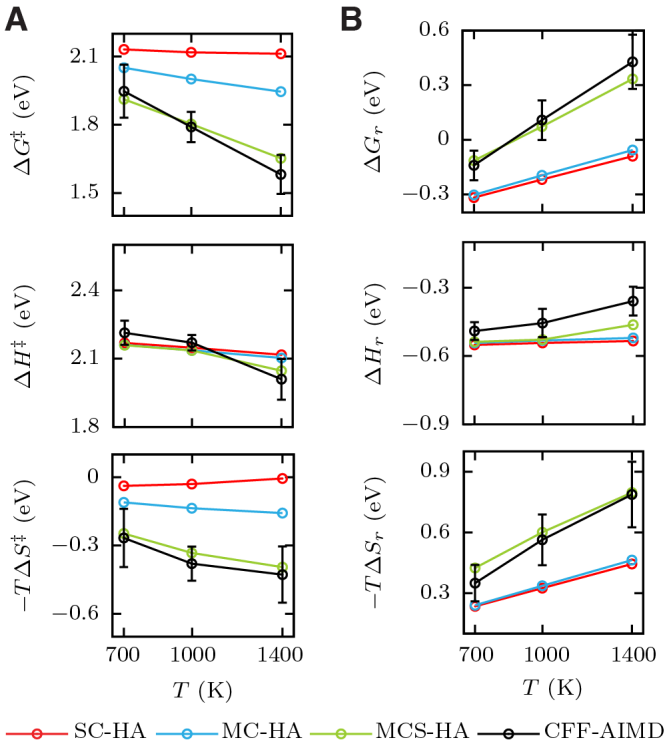


**Figure 5.** Comparison of thermodynamic quantities computed using CFF-AIMD and several different HA methods (SC-, MC-, and MCS-HA). (A) Effect of temperature on the free energy (top), enthalpy (middle), and entropy (bottom) of the associative desorption of $N_2$, $\Delta E^{\ddagger} = E(\mathrm{TS}) - E(2\mathrm{N}^*)$. (B) Same as panel (A) but on the surface reaction energy, $\Delta E_r = E(2\mathrm{N}^*) - E(\mathrm{N_2}^*)$. The largest deviations between the two methods are seen using SC-HA. There is a good agreement between MCS-HA and CFF-AIMD, showing that additional temperature-dependent effects captured by CFF-AIMD can be explained by configurational degeneracy, thermal averaging of multiple adsorbed states, and vibrational entropy of surface atoms.

Similar to previous DFT studies of molecular dissociation on metal surfaces,[6] we first consider HA calculations using the single lowest-energy configuration for each state ($N_2$*, TS, and 2N*) and only the normal modes of the adsorbate (*i.e.*, adsorbed N atoms) without the surface atoms. This is the most conventional usage of HA in the context of surface science, and we term this approach "single configuration HA" (SC-HA). As shown in Figure 5, there are large deviations in free energies between SC-HA and CFF-AIMD in the associative desorption barrier and the surface reaction energy, which are also statistically significant. Surprisingly, the two methods predict opposite trends for the temperature-dependence of $\Delta S^{\ddagger}(T)$. The $T\Delta S^{\ddagger}(T)$ term is nearly zero and shows a decreasing trend with temperature in SC-HA, while it is much greater than zero and increases with increasing temperature in CFF-AIMD.

There are several possible sources of entropic effects beyond SC-HA in CFF-AIMD, including the anharmonicity, configurational entropy of adsorbates, and vibrational entropy due to mobile surface atoms. The analysis on vibrational anharmonicity demonstrates that 2N*, $N_2$*, and TS states are mostly harmonic (Figure S5), though there can be other types of anharmonicity, such as the rotational entropy. Based on multiple 2N* states observed in CFF-AIMD simulations, we consider an ensemble of adsorbate configurations in HA, which we refer to as "multiple configuration HA (MC-HA)" (see Supporting Information). As illustrated in Figure 3, CFF-AIMD demonstrates better agreement in $\Delta G^{\ddagger}(T)$ with MC-HA than with SC-HA, especially in the temperature-dependence of $\Delta S^{\ddagger}(T)$. However, there is a minor change in $\Delta S_r(T)$ between MC-HA and SC-HA because configurational entropies of $N_2$* and 2N* states are comparable. To understand the remaining discrepancy between HA and CFF-AIMD, we include the vibrational entropy from both the nitrogen and the mobile surface atoms in the HA, called "multiple configurations with surface atoms (MCS-HA)" (see Supporting Information). For our 2x2

supercell of the Ru(0001) surface, we consider the surface phonons at the $\bar{\Gamma}$ point, which also effectively includes boundary points of the surface Brillouin zone of the primitive cell (see Supporting Information for discussion on surface phonon modes). Comparing MCS-HA and CFF-AIMD results, we find a good agreement between the two methods even at higher temperatures. This finding shows that the change in vibrational entropy of the surface atoms in elementary reactions can be substantial, although this effect is often neglected in studies of reactions on transition metal surfaces.

We computed the free energy landscape of a prototypical metal catalyzed reaction, the dissociation of $N_2$ on Ru(0001), using a neural network-based enhanced sampling method, CFF-AIMD. Our neural network-based method adaptively refines under-visited regions of the FES by estimating the mean forces and frequencies of visits, thus accelerating the enhanced sampling simulations. We find that the PMF for the adsorbed $N_2$ dissociating on the metal contains two minima with a narrow transition pathway, and that the energetic barriers are consistent with experiments. The predicted enthalpic energy surface shows that a previously reported flat-lying molecularly adsorbed state is absent in the FES, but is present in the PES. This phenomenon demonstrates the value of enhanced sampling methods, which self-consistently identify critical points on the FES, unlike conventional HA approaches, which compute free energies using critical points determined from other PES-based methods. Results from several variants of HA reveal that there are significant deviations in temperature-dependent thermodynamic quantities between CFF-AIMD and the standard HA because of the configurational entropy, thermal averaging of multiple states, the surface atom vibrational modes, and possible anharmonic contributions. Among these effects, the largest contribution to the reaction free energies and barriers is the vibrational entropy of surface atoms. These findings suggest that accelerated AIMD simulations can directly compute

the underlying FES that governs the reaction and identify the critical points on the FES required to understand reactions with entropic effects and multiple degrees of freedom.

Generalizable, efficient free energy methods are key for studying surface reactions that exhibit appreciable entropic effects to reaction energies, such as those involving large adsorbates, solvent-electrolyte species, and soft or porous surfaces such as MOFs. Machine learning-assisted enhanced sampling approaches, such as CFF-AIMD, can discover and elucidate the reaction mechanisms for these complex systems.

## COMPUTATIONAL METHODS

*System Setup*. DFT was used to model $N_2$ dissociation reaction on Ru(0001). DFT calculations were carried out using the Perdew-Burke-Ernzerhof (PBE) exchange-correlational functional[62] as implemented in the Qbox code.[63,64] The system was modeled as a nitrogen molecule on a 2x2 unit cell of two-layer Ru(0001) slab with periodic boundary condition in 3D (Figure 1A). A vacuum spacing of 10 Å in the direction normal to the surface plane was included to avoid interaction across periodic images. The top layer of surface atoms are unfixed; this allows for thermal motion of surface atoms during the reaction. The atoms in the bottom surface layer were held fixed at their equilibrium positions with lattice constants determined by optimizing the bulk lattice. The ion cores were described using Optimized Norm-Conserving Vanderbilt pseudopotentials from the SG15 library[65,66], and a plane-wave basis for the valence electrons was used with an energy cutoff of 50 Ry, $2 \times 2 \times 1$ $k$-point mesh, and Fermi smearing with electronic temperature of 1090 K. PBE tends to over-bind adsorbates to surfaces by a few tenths of eV[57], and combined with our DFT benchmark studies (Supporting Information), an overall DFT error in predicted barriers can be on the order of tenths of eV.

*Enhanced Sampling Simulations*. CFF-AIMD[45] and ABF-AIMD[67] were used to compute the PMF or the FES for the dissociation reaction using the SSAGES software package[68,69] coupled to the AIMD software Qbox. Unbiased AIMD and enhanced sampling simulations (CFF-AIMD and ABF-AIMD) were performed at the NVT ensemble using the Bussi-Donadio-Parrinello thermostat[70] with a time step of 0.483 fs at each temperature setting (700 K, 1000 K, and 1400 K). Adsorbate complexes with varying N-N bond lengths were equilibrated at finite temperature using 5 ps-long unbiased AIMD simulations, resulting in multiple configurations of $N_2$* and 2N* states. These configurations were used to initialize individual walkers in CFF-AIMD and ABF-AIMD simulations. Two CVs (*r, Z*) were chosen to compute free energies (Figure 1A). A 2D non-rectangular CV grid is used to avoid unphysical, high energy regions (> 4 eV) (Figure S7). CFF-AIMD simulations employed BRANNs with two hidden layers (14 and 10 nodes in the first and second layers, respectively). Our benchmark studies show that the performance is insensitive to the neural network architecture as long the network size is sufficiently large, and the Bayesian regularization reduces the risk of overfitting (see the Supporting Information and Figure S6). The FES was evaluated by integrating mean forces over the CV grid to directly compare CFF-AIMD and ABF-AIMD. To provide statistical uncertainties of the PMF, we averaged over three independent enhanced sampling simulations and calculated the standard deviation. Descriptions of CFF-AIMD simulations are in the Supporting Information.

*Harmonic Approximation*. In free energy calculations using HA, initial and final states of the reaction were determined using energy minimization, and transition states were identified via the fixed bond length method,[71] which was benchmarked against the climbing image nudge elastic band method.[72] The thermochemistry module in the Atomic Simulation Environment (ASE)[73] was used to perform temperature-dependent corrections to energies of adsorbed states (HA) and the

gas phase (ideal gas approximation at pressure of 150 bar). Supporting Information includes descriptions of HA and transition state search calculations.

ASSOCIATED CONTENT

**Supporting Information**. The following files are available free of charge. DFT description and benchmark, transition state search calculations, descriptions of HA and CFF methods, free energy calculations using CFF-AIMD, neural network sensitivity analysis, discussion on sampling using ABF-AIMD, calculations of entropy and enthalpy, anharmonicity analysis, calculation of the tilt angle distribution, and adsorption site analysis (PDF link)

Movie S1: Reaction of $N_2$* to 2N* on Ru(0001) from an CFF-AIMD simulation at 700 K

ACKNOWLEDGMENT

We thank Alan C. Luntz for helpful discussions. E.M.Y.L. thanks Alvin Yu for a careful reading of the manuscript and providing scientific commentary. This work is supported by the Midwest Integrated Center for Computational Materials (MICCoM) as part of the Computational Materials Sciences Program funded by the U.S. Department of Energy, Office of Science, Basic Energy Sciences, Materials Sciences and Engineering Division, through Argonne National Laboratory, under Contract No. DE-AC02-06CH11357. T.L., A.R.S., and J.K.N. acknowledge support from the SUNCAT Center for Interface Science and Catalysis as part of the U.S. Department of Energy, Office of Science, Office of Basic Energy Sciences, Chemical Sciences, Geosciences, and Biosciences Division, Catalysis Science Program; and Villum Fonden, part of the Villum Center for the Science of Sustainable Fuels and Chemicals (V-SUSTAIN grant 9455). T.L. acknowledges support from the US Department of Energy through the Computational Sciences Graduate Fellowship (DOE CSGF) under grant number DE-FG02-97ER25308. This research used

computing resources provided by Bebop, a high-performance computing cluster operated by the Laboratory Computing Resource Center (LCRC) at Argonne National Laboratory; the University of Chicago Research Computing Center (RCC); Stanford Research Computing Center (SRCC); and the National Energy Research Scientific Computing Center (NERSC) supported by the Office of Science of the U.S. Department of Energy under Contract No. DE-AC02-05CH11231.

REFERENCES

(1) Nørskov, J. K.; Abild-Pedersen, F.; Studt, F.; Bligaard, T. Density Functional Theory in Surface Chemistry and Catalysis. *Proc. Natl. Acad. Sci. U.S.A.* **2011**, *108* (3), 937–943.
(2) Nørskov, J. K.; Studt, F.; Abild-Pedersen, F.; Bligaard, T. Fundamental Concepts in Heterogeneous Catalysis; 2014.
(3) Lansford, J. L.; Vlachos, D. G. Infrared Spectroscopy Data- and Physics-Driven Machine Learning for Characterizing Surface Microstructure of Complex Materials. *Nat. Commun.* **2020**, *11* (1), 1513.
(4) Pattabathula, V.; Richardson, J. Introduction to Ammonia Production. *CEP Magazine*. 2016, pp 69–75.
(5) Liu, H. Ammonia Synthesis Catalyst 100 Years: Practice, Enlightenment and Challenge. *Chinese J. Catal.* **2014**, *35* (10), 1619–1640.
(6) Honkala, K.; Hellman, A.; Remediakis, I. N.; Logadottir, A.; Carlsson, A.; Dahl, S.; Christensen, C. H.; Nørskov, J. K. Ammonia Synthesis from First-Principles Calculations. *Science* **2005**, *307* (5709), 555–558.
(7) Shi, H.; Jacobi, K.; Ertl, G. Dissociative Chemisorption of Nitrogen on Ru(0001). *J. Chem. Phys.* **1993**, *99* (11), 9248–9254.
(8) Romm, L.; Katz, G.; Kosloff, R.; Asscher, M. Dissociative Chemisorption of $N_2$ on Ru(001) Enhanced by Vibrational and Kinetic Energy: Molecular Beam Experiments and Quantum Mechanical Calculations. *J. Phys. Chem. B* **1997**, *101* (12), 2213–2217.
(9) Murphy, M. J.; Skelly, J. F.; Hodgson, A.; Hammer, B. Inverted Vibrational Distributions from $N_2$ Recombination at Ru(001): Evidence for a Metastable Molecular Chemisorption Well. *J. Chem. Phys.* **1999**, *110* (14), 6954–6962.
(10) Diekhöner, L.; Mortensen, H.; Baurichter, A.; Luntz, A. C. Coverage Dependence of Activation Barriers: Nitrogen on Ru(0001). *J. Vac. Sci. Technol. A* **2000**, *18* (4), 1509–1513.
(11) Dietrich, H.; Geng, P.; Jacobi, K.; Ertl, G. Sticking Coefficient for Dissociative Adsorption of $N_2$ on Ru Single-crystal Surfaces. *J. Chem. Phys.* **1996**, *104* (1), 375–381.
(12) Diekhöner, L.; Mortensen, H.; Baurichter, A.; Luntz, A. C. Laser Assisted Associative Desorption of $N_2$ and CO from Ru(0001). *J. Chem. Phys.* **2001**, *115* (7), 3356–3373.
(13) Hammer, B.; Nørskov, J. K. Theoretical Surface Science and Catalysis—Calculations and Concepts. In *Advances in Catalysis*; Impact of Surface Science on Catalysis; Academic Press, 2000; Vol. 45, pp 71–129.

(14) Mortensen, J. J.; Morikawa, Y.; Hammer, B.; Nørskov, J. K. Density Functional Calculations of $N_2$ Adsorption and Dissociation on a Ru(0001) Surface. *J. Catal.* **1997**, *169* (1), 85–92.
(15) Shakouri, K.; Behler, J.; Meyer, J.; Kroes, G.-J. Accurate Neural Network Description of Surface Phonons in Reactive Gas–Surface Dynamics: $N_2$ + Ru(0001). *J. Phys. Chem. Lett.* **2017**, *8* (10), 2131–2136.
(16) Spiering, P.; Shakouri, K.; Behler, J.; Kroes, G.-J.; Meyer, J. Orbital-Dependent Electronic Friction Significantly Affects the Description of Reactive Scattering of $N_2$ from Ru(0001). *J. Phys. Chem. Lett.* **2019**, *10* (11), 2957–2962.
(17) Díaz, C.; Vincent, J. K.; Krishnamohan, G. P.; Olsen, R. A.; Kroes, G. J.; Honkala, K.; Nørskov, J. K. Multidimensional Effects on Dissociation of $N_2$ on Ru(0001). *Phys. Rev. Lett.* **2006**, *96* (9), 096102.
(18) Mortensen, J. J.; Hammer, B.; Nørskov, J. K. Alkali Promotion of $N_2$ Dissociation over Ru(0001). *Phys. Rev. Lett.* **1998**, *80* (19), 4333–4336.
(19) Dahl, S.; Logadottir, A.; Egeberg, R. C.; Larsen, J. H.; Chorkendorff, I.; Törnqvist, E.; Nørskov, J. K. Role of Steps in $N_2$ Activation on Ru(0001). *Phys. Rev. Lett.* **1999**, *83* (9), 1814–1817.
(20) Riss, A.; Paz, A. P.; Wickenburg, S.; Tsai, H.-Z.; De Oteyza, D. G.; Bradley, A. J.; Ugeda, M. M.; Gorman, P.; Jung, H. S.; Crommie, M. F.; Rubio, A.; Fischer, F. R. Imaging Single-Molecule Reaction Intermediates Stabilized by Surface Dissipation and Entropy. *Nat. Chem.* **2016**, *8* (7), 678–683.
(21) Sauer, J. Ab Initio Calculations for Molecule–Surface Interactions with Chemical Accuracy. *Acc. Chem. Res.* **2019**, *52* (12), 3502–3510.
(22) Sun, J.-J.; Cheng, J. Solid-to-Liquid Phase Transitions of Sub-Nanometer Clusters Enhance Chemical Transformation. *Nat. Commun.* **2019**, *10* (1), 5400.
(23) Collinge, G.; Yuk, S. F.; Nguyen, M.-T.; Lee, M.-S.; Glezakou, V.-A.; Rousseau, R. Effect of Collective Dynamics and Anharmonicity on Entropy in Heterogenous Catalysis: Building the Case for Advanced Molecular Simulations. *ACS Catal.* **2020**, 9236–9260.
(24) Flaherty, D. W.; Iglesia, E. Transition-State Enthalpy and Entropy Effects on Reactivity and Selectivity in Hydrogenolysis of n-Alkanes. *J. Am. Chem. Soc.* **2013**, *135* (49), 18586–18599.
(25) Amsler, J.; Plessow, P. N.; Studt, F.; Bučko, T. Anharmonic Correction to Adsorption Free Energy from DFT-Based MD Using Thermodynamic Integration. *J. Chem. Theory Comput.* **2021**, *17*, 1155-1169.
(26) Jiang, B.; Li, J.; Guo, H. High-Fidelity Potential Energy Surfaces for Gas-Phase and Gas–Surface Scattering Processes from Machine Learning. *J. Phys. Chem. Lett.* **2020**. *11*, 5120-5131.
(27) Sengul, M. Y.; Randall, C. A.; van Duin, A. C. T. ReaxFF Molecular Dynamics Study on the Influence of Temperature on Adsorption, Desorption, and Decomposition at the Acetic Acid/Water/ZnO($10\bar{1}0$) Interface Enabling Cold Sintering. *ACS Appl. Mater. Interfaces* **2018**, *10* (43), 37717–37724.
(28) Senftle, T. P.; Hong, S.; Islam, M. M.; Kylasa, S. B.; Zheng, Y.; Shin, Y. K.; Junkermeier, C.; Engel-Herbert, R.; Janik, M. J.; Aktulga, H. M.; Verstraelen, T.; Grama, A.; van Duin, A. C. T. The ReaxFF Reactive Force-Field: Development, Applications and Future Directions. *npj Comput. Mater.* **2016**, *2* (1), 15011.

(29) Bussi, G.; Laio, A. Using Metadynamics to Explore Complex Free-Energy Landscapes. *Nature Reviews Physics* **2020**, *2* (4), 200–212.
(30) Comer, J.; Gumbart, J. C.; Hénin, J.; Lelièvre, T.; Pohorille, A.; Chipot, C. The Adaptive Biasing Force Method: Everything You Always Wanted To Know but Were Afraid To Ask. *J. Phys. Chem. B* **2015**, *119* (3), 1129–1151.
(31) Sun, G.; Jiang, H. Ab Initio Molecular Dynamics with Enhanced Sampling for Surface Reaction Kinetics at Finite Temperatures: $CH_2 \rightleftharpoons CH + H$ on Ni(111) as a Case Study. *J. Chem. Phys.* **2015**, *143* (23), 234706.
(32) Herron, J. A.; Morikawa, Y.; Mavrikakis, M. Ab Initio Molecular Dynamics of Solvation Effects on Reactivity at Electrified Interfaces. *Proc. Natl. Acad. Sci. U.S.A.* **2016**, *113* (34), E4937–E4945.
(33) Cheng, T.; Xiao, H.; Goddard, W. A. Full Atomistic Reaction Mechanism with Kinetics for CO Reduction on Cu(100) from Ab Initio Molecular Dynamics Free-Energy Calculations at 298 K. *Proc. Natl. Acad. Sci. U.S.A.* **2017**, *114* (8), 1795–1800.
(34) Kristoffersen, H. H.; Chan, K.; Vegge, T.; Hansen, H. A. Energy–Entropy Competition in Cation–Hydroxyl Interactions at the Liquid Water–Pt(111) Interface. *Chem. Commun.* **2020**, *56* (3), 427–430.
(35) Martínez-Suárez, L.; Siemer, N.; Frenzel, J.; Marx, D. Reaction Network of Methanol Synthesis over Cu/ZnO Nanocatalysts. *ACS Catal.* **2015**, *5* (7), 4201–4218.
(36) Réocreux, R.; Michel, C.; Fleurat-Lessard, P.; Sautet, P.; Steinmann, S. N. Evaluating Thermal Corrections for Adsorption Processes at the Metal/Gas Interface. *J. Phys. Chem. C* **2019**, *123* (47), 28828–28835.
(37) Guo, C.; Wang, Z.; Wang, D.; Wang, H.-F.; Hu, P. First-Principles Determination of CO Adsorption and Desorption on Pt(111) in the Free Energy Landscape. *J. Phys. Chem. C* **2018**, *122* (37), 21478–21483.
(38) Réocreux, R.; Girel, É.; Clabaut, P.; Tuel, A.; Besson, M.; Chaumonnot, A.; Cabiac, A.; Sautet, P.; Michel, C. Reactivity of Shape-Controlled Crystals and Metadynamics Simulations Locate the Weak Spots of Alumina in Water. *Nat. Commun.* **2019**, *10* (1), 3139.
(39) Foppa, L.; Iannuzzi, M.; Copéret, C.; Comas-Vives, A. Adlayer Dynamics Drives CO Activation in Ru-Catalyzed Fischer–Tropsch Synthesis. *ACS Catal.* **2018**, *8* (8), 6983–6992.
(40) Ludwig, T.; Singh, A. R.; Nørskov, J. K. Subsurface Nitrogen Dissociation Kinetics in Lithium Metal from Metadynamics. *J. Phys. Chem. C* **2020**, *124*, 26368-26378.
(41) Bernardi, R. C.; Melo, M. C. R.; Schulten, K. Enhanced Sampling Techniques in Molecular Dynamics Simulations of Biological Systems. *Biochim. Biophys. Acta.* **2015**, *1850* (5), 872–877.
(42) Yu, A.; Lee, E. M. Y.; Jin, J.; Voth, G. A. Atomic-Scale Characterization of Mature HIV-1 Capsid Stabilization by Inositol Hexakisphosphate (IP6). *Sci. Adv.* **2020**, *6*, eabc6465.
(43) Yu, A.; Lau, A. Y. Energetics of Glutamate Binding to an Ionotropic Glutamate Receptor. *J. Phys. Chem. B* **2017**, *121* (46), 10436–10442.
(44) Guo, A. Z.; Sevgen, E.; Sidky, H.; Whitmer, J. K.; Hubbell, J. A.; de Pablo, J. J. Adaptive Enhanced Sampling by Force-Biasing Using Neural Networks. *J. Chem. Phys.* **2018**, *148* (13), 134108.
(45) Sevgen, E.; Guo, A. Z.; Sidky, H.; Whitmer, J. K.; de Pablo, J. J. Combined Force-Frequency Sampling for Simulation of Systems Having Rugged Free Energy Landscapes. *J. Chem. Theory Comput.* **2020**, *16* (3), 1448–1455.

(46) Sidky, H.; Whitmer, J. K. Learning Free Energy Landscapes Using Artificial Neural Networks. *J. Chem. Phys.* **2018**, *148* (10), 104111.
(47) Zhang, J.; Yang, Y. I.; Noé, F. Targeted Adversarial Learning Optimized Sampling. *J. Phys. Chem. Lett.* **2019**, *10* (19), 5791–5797.
(48) Bonati, L.; Zhang, Y.-Y.; Parrinello, M. Neural Networks-Based Variationally Enhanced Sampling. *Proc. Natl. Acad. Sci. U.S.A.* **2019**, *116* (36), 17641–17647.
(49) Zhang, L.; Wang, H.; E, W. Reinforced Dynamics for Enhanced Sampling in Large Atomic and Molecular Systems. *J. Chem. Phys.* **2018**, *148* (12), 124113.
(50) Mones, L.; Bernstein, N.; Csányi, G. Exploration, Sampling, And Reconstruction of Free Energy Surfaces with Gaussian Process Regression. *J. Chem. Theory Comput.* **2016**, *12* (10), 5100–5110.
(51) Henkelman, G.; Jónsson, H. Improved Tangent Estimate in the Nudged Elastic Band Method for Finding Minimum Energy Paths and Saddle Points. *J. Chem. Phys.* **2000**, *113* (22), 9978–9985.
(52) Halstead, D.; Holloway, S. The Influence of Potential Energy Surface Topologies on the Dissociation of $H_2$. *J. Chem. Phys.* **1990**, *93* (4), 2859–2870.
(53) Hammer, B.; Scheffler, M.; Jacobsen, K. W.; Nørskov, J. K. Multidimensional Potential Energy Surface for H 2 Dissociation over Cu(111). *Phys. Rev. Lett.* **1994**, *73* (10), 1400–1403.
(54) Ong, S. P.; Richards, W. D.; Jain, A.; Hautier, G.; Kocher, M.; Cholia, S.; Gunter, D.; Chevrier, V. L.; Persson, K. A.; Ceder, G. Python Materials Genomics (Pymatgen): A Robust, Open-Source Python Library for Materials Analysis. *Comput. Mater. Sci.* **2013**, *68*, 314–319.
(55) Montoya, J. H.; Persson, K. A. A High-Throughput Framework for Determining Adsorption Energies on Solid Surfaces. *npj Comput. Mater.* **2017**, *3* (1), 1–4.
(56) Mallikarjun Sharada, S.; Bligaard, T.; Luntz, A. C.; Kroes, G.-J.; Nørskov, J. K. SBH10: A Benchmark Database of Barrier Heights on Transition Metal Surfaces. *J. Phys. Chem. C* **2017**, *121* (36), 19807–19815.
(57) Wellendorff, J.; Lundgaard, K. T.; Møgelhøj, A.; Petzold, V.; Landis, D. D.; Nørskov, J. K.; Bligaard, T.; Jacobsen, K. W. Density Functionals for Surface Science: Exchange-Correlation Model Development with Bayesian Error Estimation. *Phys. Rev. B* **2012**, *85* (23), 235149.
(58) Gerrits, N.; Smeets, E. W. F.; Vuckovic, S.; Powell, A. D.; Doblhoff-Dier, K.; Kroes, G.-J. Density Functional Theory for Molecule–Metal Surface Reactions: When Does the Generalized Gradient Approximation Get It Right, and What to Do If It Does Not. *J. Phys. Chem. Lett.* **2020**, *11* (24), 10552–10560.
(59) Dumesic, J. A.; Rudd, D. F.; Aparicio, L. M.; Rekoske, J. E.; Treviño, A. A. *The Microkinetics of Heterogeneous Catalysis*, 1st Edition.; American Chemical Society: Washington, DC, 1993.
(60) Murphy, M. J.; Samson, P.; Skelly, J. F.; Hodgson, A. Product State Measurements of Nitrogen Formation at Surfaces. In *Atomic and Molecular Beams: The State of the Art 2000*; Campargue, R., Ed.; Springer Berlin Heidelberg: Berlin, Heidelberg, 2001; pp 887–900.
(61) Bowker, M. The Role of Precursor States in Adsorption, Surface Reactions and Catalysis. *Top Catal.* **2016**, *59* (8), 663–670.
(62) Perdew, J. P.; Burke, K.; Ernzerhof, M. Generalized Gradient Approximation Made Simple. *Phys. Rev. Lett.* **1996**, *77* (18), 3865–3868.

(63) Gygi, F. Architecture of Qbox: A Scalable First-Principles Molecular Dynamics Code. *IBM J. Res. Dev.* **2008**, *52* (1.2), 137–144.
(64) Qbox First-Principles Molecular Dynamics Code http://qboxcode.org (accessed Jul 13, 2019).
(65) Schlipf, M.; Gygi, F. Optimization Algorithm for the Generation of ONCV Pseudopotentials. *Comput. Phys. Commun.* **2015**, *196*, 36–44.
(66) Hamann, D. R. Optimized Norm-Conserving Vanderbilt Pseudopotentials. *Phys. Rev. B* **2013**, *88* (8), 085117.
(67) Darve, E.; Rodríguez-Gómez, D.; Pohorille, A. Adaptive Biasing Force Method for Scalar and Vector Free Energy Calculations. *J. Chem. Phys.* **2008**, *128* (14), 144120.
(68) Sidky, H.; Colón, Y. J.; Helfferich, J.; Sikora, B. J.; Bezik, C.; Chu, W.; Giberti, F.; Guo, A. Z.; Jiang, X.; Lequieu, J.; Li, J.; Moller, J.; Quevillon, M. J.; Rahimi, M.; Ramezani-Dakhel, H.; Rathee, V. S.; Reid, D. R.; Sevgen, E.; Thapar, V.; Webb, M. A.; Whitmer, J. K.; de Pablo, J. J. SSAGES: Software Suite for Advanced General Ensemble Simulations. *J. Chem. Phys.* **2018**, *148* (4), 044104.
(69) SSAGES: Software Suite for Advanced General Ensemble Simulations https://ssagesproject.github.io/ (accessed Jun 15, 2020).
(70) Bussi, G.; Donadio, D.; Parrinello, M. Canonical Sampling through Velocity Rescaling. *J. Chem. Phys.* **2007**, *126* (1), 014101.
(71) Alavi, A.; Hu, P.; Deutsch, T.; Silvestrelli, P. L.; Hutter, J. CO Oxidation on Pt(111): An *Ab Initio* Density Functional Theory Study. *Phys. Rev. Lett.* **1998**, *80* (16), 3650–3653.
(72) Henkelman, G.; Uberuaga, B. P.; Jónsson, H. A Climbing Image Nudged Elastic Band Method for Finding Saddle Points and Minimum Energy Paths. *J. Chem. Phys.* **2000**, *113* (22), 9901–9904.
(73) Hjorth Larsen, A.; Jørgen Mortensen, J.; Blomqvist, J.; Castelli, I. E.; Christensen, R.; Dułak, M.; Friis, J.; Groves, M. N.; Hammer, B.; Hargus, C.; Hermes, E. D.; Jennings, P. C.; Bjerre Jensen, P.; Kermode, J.; Kitchin, J. R.; Leonhard Kolsbjerg, E.; Kubal, J.; Kaasbjerg, K.; Lysgaard, S.; Bergmann Maronsson, J.; Maxson, T.; Olsen, T.; Pastewka, L.; Peterson, A.; Rostgaard, C.; Schiøtz, J.; Schütt, O.; Strange, M.; Thygesen, K. S.; Vegge, T.; Vilhelmsen, L.; Walter, M.; Zeng, Z.; Jacobsen, K. W. The Atomic Simulation Environment-a Python Library for Working with Atoms. *J. Phys. Condens. Matter.* **2017**, *29* (27), 273002.